Tutor/s

Dra. Montserrat Corbella Cordomí
Departament de Química Inorgànica

Dr. Gerard Tobias Rossell
ICMAB - CSIC

Grau de Química

Treball Final de Grau

Sustainable synthesis of Metal-Organic Frameworks (MOF).
Síntesis sostenible de Metal-Organic Frameworks (MOF).

Pedro López Domínguez

June 2015

Universitat de Barcelona

Campus d'Excel·lència Internacional
BKC Barcelona Knowledge Campus

It's kind of fun to do the impossible

Walt Disney

Grazas aos meus pais, por saber espertar en min a curiosidade polas cousas. A vós débovos todos os valores que me fan crecer como persoa.

A mi tutora, por atenderme siempre con esa vitalidad contagiosa. A toda la gente del CSIC, y en especial a Ana por ser mi guía en esta nueva etapa. Gracias por dejar volar mi imaginación. También a Concha, Gerard, Jorge y a mis compañeros de despacho por todas las buenas horas compartidas.

Y gracias también a todos aquellos que aunque no nombre, me han acompañado y han formado parte de este maravilloso viaje.

REPORT

CONTENTS

1. SUMMARY 3
2. RESUMEN 5
3. INTRODUCTION 7
3.1. Porous materials 7
3.2. Metal-organic frameworks 8
3.2.1. HKUST-1 9
3.2.2. ZIF-8 10
3.3. Supercritical CO_2 as a green solvent 12
4. CHARACTERIZATION TECHNIQUES 14
4.1. X-ray powder diffraction 14
4.2. Thermal analysis 15
4.3. Scanning electron microscopy 16
4.4. Textural properties – Surface area determination 16
4.5. Elemental analysis 18
5. OBJECTIVES 19
6. EXPERIMENTAL SECTION 20
6.1. Supercritical CO_2 processing equipment 20
6.2. Supercritical method. General considerations 22
6.3. Preparation of MOFs 22
6.3.1. Preparation of HKUST-1 ($Cu_3(BTC)_2 \cdot 3H_2O$) 23
6.3.2. Preparation of ZIF-8 ($Zn(2\text{-mIm})_2$) 23
7. RESULTS AND DISCUSSION 24
7.1. Characterization of HKUST-1 24
7.1.1. X-ray diffraction 24
7.1.2. Thermogravimetric analysis 25
7.1.3. Scanning electron microscopy 26

7.1.4. Surface area and pore distribution 28
7.2. Characterization of ZIF-8 29
7.2.1. X-ray diffraction 29
7.2.2. Thermogravimetric analysis 30
7.2.3. Scanning electron microscopy 31
7.2.4. Surface area and pore distribution 32
7.3. Colour change in HKUST-1 33
7.3.1. Experimental observations. Introduction 33
7.3.2. Analysis of crystal field splitting diagrams 35
8. CONCLUSIONS 39
9. REFERENCES AND NOTES 41
10. ACRONYMS 43

1. SUMMARY

The research presented in this work investigates the use of green solvents in the synthesis of a new-class of hybrid porous materials, named metal-organic frameworks (MOFs), which are formed by the combination of metallic centres and organic linkers. The fluid technology based on supercritical carbon dioxide ($scCO_2$) has been studied as a promising alternative for safer and cleaner synthesis over the conventional solvothermal conditions. In particular, the specific goal stablished for this research is to successfully synthesize two widely-known compounds with MOF structures denominated HKUST-1 and ZIF-8 that will demonstrate the applicability of the method. The reactions were carried out in a reactor vessel at the conditions of 200 bar, 70 ºC for 20 hours in a medium of $scCO_2$ with selected additives. The reactant quantities were used in stoichiometric ratios according to the formula unit of each MOF. The physicochemical and textural properties of the prepared samples were measured and compared to those obtained from conventional methods. The two products have been successfully synthesized with a high-degree of purity as demonstrated by the elemental analysis. The structure of HKUST-1 corresponds to a face-centred cubic lattice with an observed surface area of 1290 $m^2 \cdot g^{-1}$, in accordance with previous reported data. ZIF-8 was also obtained with the same structure than the one described in the literature, but with outstanding values of surface area (1730 $m^2 \cdot g^{-1}$), which overpass most of the values reported with other synthetic approaches. In the last part of this report, an explanation based on the ultraviolet-visible (UV-Vis) spectra and the Crystal Field Theory is provided as a tool to understand the observed colour change in HKUST-1.

Keywords: Green chemistry, supercritical CO_2, MOF, porous materials, hybrid products.

2. RESUMEN

Este trabajo recoge la investigación realizada con el fin de incorporar los disolventes verdes en la síntesis de una nueva clase de materiales porosos híbridos llamados *metal-organic frameworks* (MOFs), cuya estructura se basa en centros metálicos unidos por ligandos orgánicos. Se ha estudiado como posible substituto a las actuales síntesis solvotermales, la tecnología basada en dióxido de carbono supercrítico ($scCO_2$) como un método efectivo, limpio y seguro. Con el fin de demostrar su aplicabilidad, se ha fijado el objetivo de obtener utilizando $scCO_2$ dos de los compuestos más conocidos con estructura tipo MOF, el HKUST-1 y el ZIF-8. Para ello se han llevado a cabo una serie de reacciones en un reactor presurizado. Las condiciones utilizadas son: presión de 200 bares a 70 ºC y durante 20 horas, en un medio de $scCO_2$ y aditivos seleccionados. Las cantidades utilizadas de reactivos se corresponden con las que marca la relación estequiométrica de la estructura del MOF correspondiente. Las propiedades fisicoquímicas y texturales de los materiales obtenidos han sido comparadas con respecto a aquellas que se obtienen como resultado de utilizar métodos convencionales. Ambos compuestos se han sintetizado satisfactoriamente y con un alto grado de pureza, lo que queda demostrado por los resultados de los análisis elementales. La estructura del HKUST-1 se corresponde con la de una celda cúbica centrada en las caras. El producto obtenido presenta un área superficial de 1290 $m^2 \cdot g^{-1}$, resultado que se encuentra en el rango de los previamente descritos en la literatura. El ZIF-8 se obtuvo también con la estructura esperada, pero con un valor de área superficial de 1730 $m^2 \cdot g^{-1}$, superior a la mayoría de fases preparadas utilizando métodos convencionales. La última parte de este informe desarrolla una posible explicación de los cambios de color observados en el HKUST-1 cuando se somete a tratamientos de vacío, basada en el análisis de los espectros de ultravioleta-visible (UV-Vis) y aplicando la Teoría del Campo Cristalino.

Palabras clave: Química verde, CO_2 supercrítico, MOF, materiales porosos, materiales híbridos.

3. INTRODUCTION

Industry is highly interested in controlling materials porosity, due to its importance in the design of catalysts, adsorbents, membranes and ceramics. In this section, the basics about porous materials and their classification are introduced. Next, the focus is on metal-organic frameworks (MOFs). MOFs are nowadays one of the best examples in terms of designable porous materials at the molecular level. Developed over the last 20 years, MOFs have become an exciting and highly productive field of research due to their promising applications in hydrogen storage, CO_2 capture and heterogeneous catalysis, for example. In the work presented here, two of the most representative members of the MOF family (HKUST-1 and ZIF-8) have been studied. These two materials are currently available for purchase on different vendors, including Sigma-Aldrich, highlighting their prospects for industrial applications.

However, the industrial applicability and economic feasibility of MOFs are strongly related to their scale-up and production cost. Academia usually reports the synthesis of such materials with the use of expensive and non-environmentally friendly organic solvents at high temperature and for long reaction times. Supercritical carbon dioxide ($scCO_2$), fluid described in the last part of this introductory section, has become a promising alternative to be used as a solvent in many industrial processes providing a safer replacement over organic solvents. A novel green synthetic route is explored in this work as a cheap and non-toxic alternative for the preparation of MOFs.

3.1. POROUS MATERIALS

A porous material is a solid with pores (voids), for example cavities, channels or interstices that are deeper than they are wide. Voids can be employed to store, sort by molecular size acting as molecular sieving, promote catalytically chemical transformations and transport active species. The physical properties and chemical reactivity are strongly dependent on the pore structure and therefore an accurate classification of porous systems is necessary. The International Union of Pure and Applied Chemistry (IUPAC) has developed a classification based on the following parameters: [1]

- Availability to external fluid:
  - Open pores if there is a continuous channel of communication with the external surface of the solid. Some may be opened only by one end (blind, fig. 1 b, f) and other at two ends (through pores, fig. 1 e).
  - Closed pores, those totally isolated from the neighbours (fig. 1 a).
- Shape: cylindrical (fig. 1 c, f), ink-bottle (fig. b), funnel (fig. 1 d) and slit.

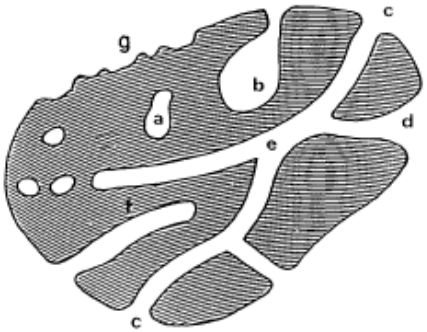

Figure 1. Schematic cross-section of a porous solid.[1]

- Size:
  - Micropores: pores smaller than 2 nm.
  - Mesopores: in the range of 2 nm to 50 nm.
  - Macropores: pores larger than 50 nm.

An alternative classification can be done attending to the chemical composition of the material:

- Organic, like covalent organic frameworks.
- Inorganic, for example, zeolites, carbon nanotubes, activated carbon, etc.
- Hybrid, comprising metal-organic frameworks.

3.2. METAL-ORGANIC FRAMEWORKS

MOFs are a class of solid materials formed by an extended network of metal ions (or clusters) coordinated to multidentate organic molecules. For a solid to be considered as metal-organic framework should display strong bonding that provides robustness, linking units available for modification by organic synthesis and geometrically well-defined structures. The

later implies that MOFs should be highly crystalline, essential for understanding their structure and properties. [2]

MOFs are normally prepared by one-pot self-assembly of metal ions or clusters (coordination centres) and organic molecules resulting in 1D, 2D and 3D structures. MOFs can exhibit ultrahigh porosity (up to 90 % free volume) and enormous surfaces areas, even beyond 6000 $m^2 \cdot g^{-1}$.[3] MOFs are normally obtained under solvothermal conditions, which involve the use of organic solvents like dimethylformamide (DMF) or diethylformamide (DEF) under high temperatures and pressures.

For classification, some metal-organic frameworks are identified by the word MOF followed by a number assigned in roughly chronological order (for example those discovered by Omar Yaghi's group like MOF-5) while others contain the name of the institution who discovered it, like MIL-53 from the Materials of Institute Lavoisier.

In this report the attention is drawn into HKUST-1 (reported first in 1999 by Chui et al.) and ZIF-8 (patented by Yaghui et al. in 2003); two of the most important metal-organic frameworks due to their structure and large number of applications.

3.2.1. HKUST-1

By far, $Cu_3(BTC)_2 \cdot 3H_2O$ (BTC=1,3,5-benzenetricarboxylate) is one of the most popular and studied metal-organic frameworks. HKUST-1 is the widespread used name for this compound, an acronym for the Hong Kong University for Science and Technology, but can also be called MOF-199. The structure of HKUST-1 is based on the coordination of the organic ligand (BTC) to copper(II) ions. The obtained material has a face-centred cubic lattice with an intersecting three-dimensional system of large square-shaped pores of size 9 x 9 Å (fig. 2).

More specifically, copper (II) ions form dimers, with a short internuclear Cu···Cu separation of 2.682 Å. Four coordination sites of each metal atom are bound to four oxygen atoms from four different linker molecules. The remaining coordination site is normally filled by a weakly bound water molecule, and thus completing the pseudooctahedral coordination sphere of the metal unit. Upon dehydration, the water molecule is lost, changing the number of coordination of copper ions from six to five. The formation of these Lewis coordination sites in the interior of the pore walls, makes copper sites accessible for catalytic conversions. [4,5]

The geometry of MOFs can also be understood by introducing the concept of Secondary Building Unit (SBU) developed by Yaghi and co-workers as an extension from the original use in zeolites. SBUs are small unities constructed from one or more metal ions and the donor atoms of multidentate linker creating well-defined entities which are repeated through the network. The arrangement in HKUST-1 is based on metal paddle-wheels (fig. 3), a SBU constructed from copper atoms bridged by four carboxylate groups from four BTC ligands. From the position of the carboxylate carbon atoms a squared shape can be defined. These atoms receive the name of points of extension as they connect to the rest of the linkers and therefore to neighbouring units. The axial positions correspond to oxygen atoms from water molecules. [6]

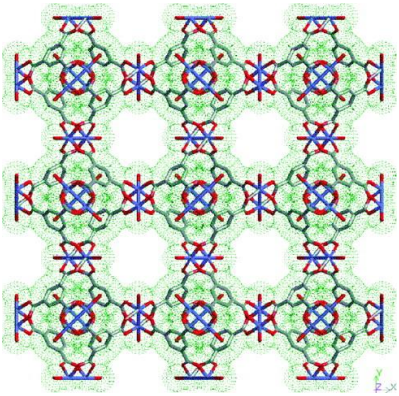

Figure 2. HKUST-1 polymer framework showing nanochannels. [5]

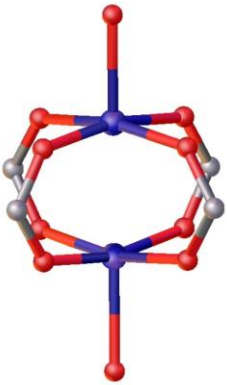

Figure 3. Copper (blue) square paddle-wheel SBU. Oxygen atoms are in red while carbon is displayed in grey (*Bosch M.et al., Advances in Chemistry,* ***2014****, ID 18232*).

HKUST-1 is nowadays produced by BASF and marketed by Sigma-Aldrich under the name of Basolite© C300

3.2.1. ZIF-8

Zeolitic Imidazolate Frameworks (ZIF) are a subclass of MOFs with similar topologies to those found in aluminosilicate zeolites. In zeolites, the framework consists of tetrahedral silicon or aluminium atoms bridged by oxygen. In ZIFs, these atoms are replaced by a transition metal and connected by imidazolate-type ligands (fig. 4). In fact, the name of ZIF arises from the

experimental observed metal-imidazolate-metal angle that it is close to that reported on zeolites (see fig. 5). ZIFs exhibit permanent porosity and exceptional chemical and thermal stabilities. [7]

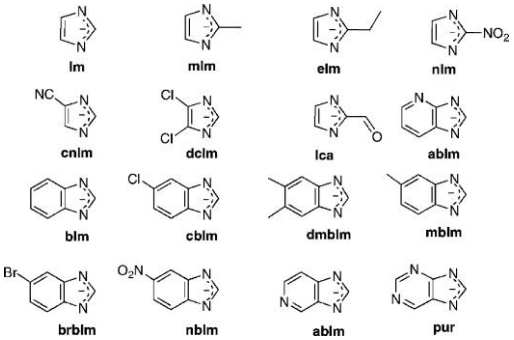

Figure 4. Typical linkers used in the construction of ZIFs. [7]

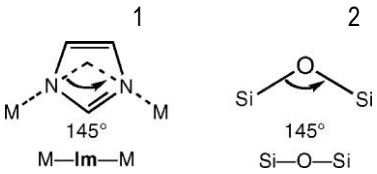

Figure 5. Bridging angles in ZIF(1) and zeolites(2). [7]

ZIF-8 is the most representative ZIF compound with a sodalite zeolite-type topology. Each zinc(II) ion is tetrahedrally coordinated to four nitrogen atoms from the ditopic bridging 2-methylimidazolate (2-mIm) to form a neutral framework with the formula unit $Zn(2\text{-mIm})_2$. The basic unit for ZIF-8 is a truncated octahedron (12.5 Å effective diameter, figure 6) accessible through hexagonal window openings of 3.3 Å in diameter. The octahedron also receives the name of cage, as the window size (pore aperture) is much smaller than the diameter of the cavity. One-dimensional channels are formed in the four directions of the cubic-lattice as a result of sharing those hexagonal faces with neighbouring cages. [7,8]

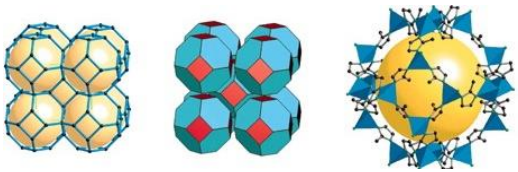

Figure 6. ZIF-8 structure shown as a stick diagram (Left), and as a tiling (Centre). (Right) The largest cage shown with ZnN_4 tetrahedron in blue. H atoms are omitted for clarity. [9]

ZIF-8 is currently produced by BASF and commercially available under the name of Basolite© Z1200.

3.3. SUPERCRITICAL CO_2 AS A GREEN SOLVENT

A supercritical fluid (SCF) is a single uniform phase obtained when a substance is pressurized and heated above its critical point. In the supercritical region, an isothermal pressure increase above the critical pressure or an isobaric temperature increase above the critical temperature maintains the fluid at supercritical conditions, without phase transition. The properties of SCF are between those of a gas and a liquid and can be tuneable with small pressure and temperature variations. Figure 7 provides the critical points for other selected fluids. [10]

Fig. 8 shows the phase diagram of carbon dioxide. The different displayed regions represent the conditions of pressure and temperature at which the various phases of CO_2 are present. A black circle points the critical point, in this case situated at 31 ºC of temperature and 7.38 MPa (73.8 bar) of pressure.

Fluid	Temperature [K]	Pressure [atm]
Hydrogen	33.23	12.8
Nitrogen	126.3	33.5
Carbon dioxide	304.2	72.8
Ammonia	405.5	111.3
Water	647.4	218.3

Figure 7. Critical point of some selected fluids. [10]

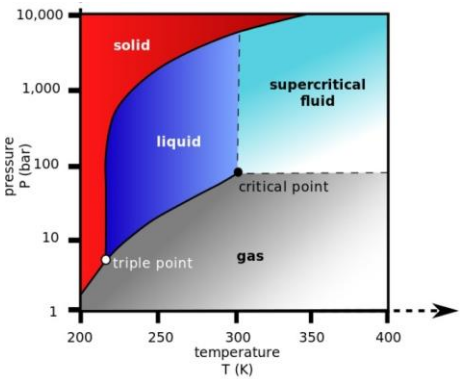

Figure 8. Phase diagram of CO_2. *(Pieter Kuiper, 25/05/15 via Wikimedia Commons, Creative Commons Attribution).*

Carbon dioxide is by far the most common solvent used in supercritical fluid processes. Its applicability as a solvent has been investigated since the 1950s. Solvents are known to play a major role in the environmental assessment of any process in the chemical industry and also on its cost, safety and health issues. Green solvents summarize the idea of minimizing the environmental impact resulting from the use of solvents in chemical production. Carbon dioxide is one of these solvents considered as “green” and a great candidate for replacing conventional

volatile organic solvents due to its exceptional physicochemical characteristics. These include its non-flammability, relatively non-toxicity, inertness and a supercritical regime readily accessible in terms of cost and equipment.

Up-to-date supercritical carbon dioxide is widely-known to be used in extraction processes, for instance the removal of caffeine from coffee beans, in Supercritical Fluid Chromatography, in nanoparticle formation, polymer processing, textile dyeing and many other examples. $scCO_2$ is also used to eliminate the solvent in silica alcogels obtaining a barely-new material called aerogel with outstanding properties, like extremely low density, high specific surface area, high porosity, high thermal insulation values, ultra-low dielectric constant and low refraction index. [11,12]

4. CHARACTERIZATION TECHNIQUES

In this section of the report, the basics about all the characterization techniques used in this investigation are summarized. Most significant information is provided by X-Ray diffraction that allows a preliminary distinction between ordered solids and amorphous materials. It also provides information about the synthesized phase and the presence of impurities by comparing the diffraction pattern from the synthesized materials with the one from the Cambridge Crystallographic Data Centre (CCDC). Once the solid has been adequately identified, a further study of its characteristics is performed with the rest of the successive techniques.

The following description includes information about the special characteristics of each techniques and the experimental details.

4.1. X-RAY POWDER DIFFRACTION

Diffraction is the phenomenon caused by the interference of an object in the path of waves that conserves the kinetic energy of the beam but changes its direction due to elastic scattering. Diffraction occurs when the dimension of the diffracting object is comparable to the wavelength of the radiation.

X-rays are electromagnetic radiation with wavelengths of the order of 10^{-10} meters. As this length is about the size of an atom, information about the size and shape of the solid unit cell can be retrieved. X-rays are typically generated by bombarding a metal (usually copper or molybdenum) with a beam of high-energy electrons emitted from a hot filament (thermionic emission). The electrons decelerate as they hit the metal and generate a radiation with a continuous range of wavelengths called broad background. Superimposed there are few high-energy sharp peaks arising from collision with electrons in the inner shells. That collision expels the electron of the inner shell, and an electron of higher energy drops into the vacancy emitting an X-ray photon. Particularly those falling in a K shell (a shell with principal quantum number, n=1) are classified as K-radiation. The X-rays are filtered to a single wavelength (monochromatic) and directed onto the sample.

The use of monochromatic radiation allows diffraction to be treated geometrically like reflection. Bragg's model of diffraction describes the condition of the incident angle for

constructive interference. Any other incident angle will result in waves out of phase and consequently a destructive interference.

$$n\lambda = 2d\ sin(\theta)$$

Here n is a positive integer, λ is the wavelength of the incident wave, d the distance between two planes of the crystal and θ the scattering angle. [10]

During this work, powder X-ray Diffraction (PXRD) has been used for the characterization of the obtained materials. Powdered samples contain randomly orientated crystallites which produce a widening of the diffraction lines. The diffractogram is obtained by recording the intensity of detected X-rays (constructive interferences) as a function of the diffraction angle (θ) and is characteristic of the sample material.

A Siemens D5000 instrument using Cu K_α incident radiation has been used for recording the diffracted X-rays from angles (2θ) in the range of 5º to 50º, with a step scan of 0.02º counting for 1 second at each step.

4.2. THERMAL ANALYSIS

Thermal analysis includes a set of techniques that measure the properties of materials as temperature changes. More specifically, thermogravimetric analysis (TGA) monitors the weight of a sample as a function of temperature under controlled atmosphere. The temperature increases with a specifically heating rate in an atmosphere prepared with synthetic air, inert gases, oxygen or even mixtures.

In MOF characterization, TGA allows the study of the stability of the synthesized phase with the possibility of locating any other thermal event that may happen during the measurement. The experimental profiles in this report were obtained with a NETZSCH-STA 449 F1 Jupiter equipment under a flow of synthetic air, with a heating rate of 10 ºC·min^{-1}, from room temperature to 700 ºC.

4.3. SCANNING ELECTRON MICROSCOPY

Scanning electron microscopy is an imaging technique based on the interaction of a high-energy electron beam with the sample. A QUANTA FEI 200 FEG-ESEM microscope was used in this work to analyse the different obtained materials. The beam is generated by applying a strong electric field to an extremely fine tungsten point (field emission). The electrons are accelerated by a voltage current between 1 and 30 kilovolts (in our case 20 kV) and focused onto the sample with electromagnetic lenses. The beam is scanned across the surface of the sample in a raster pattern. After interacting with the sample, the electrons are collected and converted into a signal that produces an image in black and white. Two kinds of electrons can be detected depending on the interaction with the sample:

- Secondary electrons (SE, inelastic scattering) give information about the shape. The yield of SE increases with decreasing the angle between the beam and the sample surface, resulting in steep surfaces and edges seen brighter than flat surfaces.
- Backscattered electrons (BSE, elastic scattering) are strongly dependent on the atomic number and thus give information about the chemical composition. In BSE images, heavy atom regions appear brighter.

In order to prevent accumulation of electrostatic charge at the surface, samples were previously coated with gold using a K550 Sputter Coater. [13,14]

4.4. TEXTURAL PROPERTIES - SURFACE AREA DETERMINATION

Specific surface area is calculated per unit of mass, and it is a significant parameter in characterizing porous materials. Surface area is commonly obtained by applying the Brunauer, Emmett and Teller (BET) theory to recorded nitrogen adsorption isotherms (changing curve of equilibrium adsorption capacity with pressure) measured at 77 K. The BET analysis relies on adsorption occurring by multilayer formation and implies that the number of adsorbed layers is infinite at the saturation pressure. BET method has been successfully proved to obtain accurate surface areas from metal-organic frameworks. [15]

Prior to the analysis, the sample is taken into a degasification process. The sample is heated under ultra-high vacuum to eliminate vapours and gases of the surface without altering

the solid. Once the instrument records all the required parameters, the analysis step starts. The instrument makes controlled additions of nitrogen into the sample tube at 77 K. Stabilized pressure (P) and adsorbed volume (V) at standard conditions (273.15 K, 1 bar) are registered.

Using a rearranged BET equation, the experimental data can be plotted like a linear equation (y = a + b·x).

$$\frac{x}{V\,(1-x)} = \overbrace{\frac{1}{C \cdot V_{mon}}}^{a} + \overbrace{\frac{C-1}{C \cdot V_{mon}}}^{b} \cdot x \qquad \textbf{\textit{where}} \quad x = \frac{P}{Ps}$$

Here V_{mon} indicates the volume of gas required for a monolayer, P_s the vapour pressure and C a constant. The range of fit for the BET equation is restricted to 0.05-0.35 for the value of P/P_s.

By using least squares regression, values for the slope (b) and intercept (a) can be calculated. After substitution to each corresponding expressions, the constant C and the volume of a monolayer are obtained. Next, the number of moles that form a monolayer is calculated by:

$$n_m = \frac{V_{mon}}{22.400}$$

And consequently surface area is given as:

$$A_s = \frac{n_m \cdot a}{m} \cdot N_A$$

The parameter 'a' stands in this case, for the nitrogen cross-sectional area ($16.2 \cdot 10^{-20}$ m^2), 'm' as the sample mass in grams and N_A as the Avogadro's number. [16]

In this work, nitrogen adsorption data were collected at 77 K (- 196 ºC) using an ASAP 2000 surface area analyser from Micromeritics Instrument Corporation. Prior to the measurements, all samples were degassed at 60 ºC for 20 h. The determination of pore size distribution (not explained in this report), was calculated using the BJH method (name taken from Barrett, Joyner and Halenda) from the adsorption isotherm. [17]

4.4. ELEMENTAL ANALYSIS

Sample content of carbon, hydrogen and nitrogen can be determined by combustion analysis. The sample is qualitatively burned at 1200 ºC in an oxygen rich current and the resulting gases are separated by gas chromatography and quantified by comparison to well-known standards.

Elemental analyses were performed at the Servei d'Analisi Química-UAB with a Thermo Scientific Flash 2000 instrument.

5. OBJECTIVES

The research presented in this work has been focused on exploring an alternative synthetic method for the preparation of porous MOFs. The following specific objectives were taken into consideration:

- To develop an effective and eco-friendly procedure for the synthesis of porous MOFs by using supercritical carbon dioxide as solvent.
- To successfully synthesize HKUST-1 and ZIF-8.
- To characterize the obtained materials by:
    - X-ray diffraction.
    - BET Surface area.
    - Thermogravimetric analysis.
    - Scanning electron microscopy.
    - Elemental analysis.

This work is subjected to a confidentiality agreement with the Institut de Ciència de Materials de Barcelona (ICMAB-CSIC) and for that reason no further information may be provided about the nature and characteristics of the used additives.

6. EXPERIMENTAL SECTION

6.1. SUPERCRITICAL CO_2 PROCESSING EQUIPMENT

Working with $scCO_2$ requires equipment suitable for high pressures and moderate temperature operation. A reactor vessel, high-pressure pump, valves, tubing, cooler, controllers and safety elements compose a standard operating equipment. Stainless steel (AISI-316) is the common material used for manufacturing those components subjected to $scCO_2$ conditions.

The engineering scheme of the equipment used for the experiments carried out in $scCO_2$ is represented in figures 9 and 10.

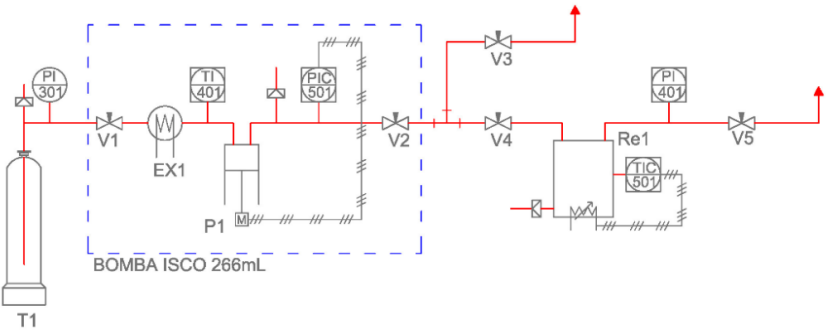

Figure 9. Supercritical equipment, engineering diagram (*extracted from García-González et al. J. Colloid Interface Sci.* ***2009,*** *338, 491-499*).

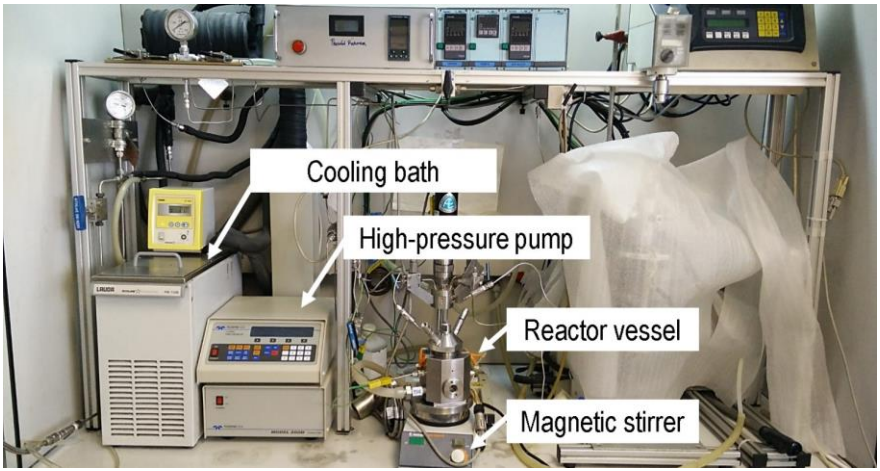

Figure 10. Supercritical equipment, picture.

The elements displayed correspond to the following devices:

- Carbon dioxide cylinder supply (T1) which is at a pressure between 5-7 MPa and at room temperature.

- Cooling system (EX1, Lauda Ecoline Staredition RE106) consisting of a bath device at a temperature of -2 ºC prepared from a 6-litre mixture of ethylene glycol and water, which had been used to liquefy the gas, so liquid CO_2 was introduced in the high pressure pump.

- A 260 mL high pressure pump (P1, Teledeyne Isco Model 260D) that pressurizes the reactor vessel. Its mechanism is based on an electrical motor that drives the syringe piston to control the outlet pressure.

- Reactor vessel (Re1) that consists of a 100 mL stainless-steel vessel (figure 11, TharDesing) equipped with two sapphire windows in opposite positions, thus allowing visual inspection of the process and the quality of stirring. The heating of the reactor is achieved with four resistance heaters placed on its corresponding cylindrical cavities made on the reactor wall.

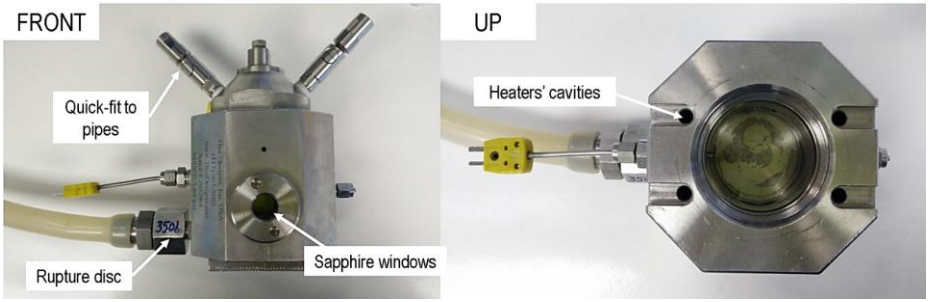

Figure 11. High-pressure reactor from TharDesign.

- High pressure valves (V1, V2, V3, V4 and V5) controlling the flow of CO_2 throughout the system. In particular, V4 is the valve that controls the flow of CO_2 entering the reactor vessel, and V5 is the valve used for depressurizing the system.

Sample stirring is provided with a magnetic stirrer (P-Selecta Agimatic E) by placing a magnetic bar inside the reactor vessel.

6.2. SUPERCRITICAL METHOD. GENERAL CONSIDERATIONS

In the general methodology used to perform an experiment under supercritical conditions, several factors and steps must be taken into account.

Working at high pressure conditions involves a strict control of the pressure and temperature parameters, being the latter of crucial importance. A sudden change in this parameter may lead to a potentially dangerous overpressure event, since the pressure rapidly increases with the temperature. For that reason, temperature and pressure must be monitored through the pressurization process and controlled all over the reaction. In addition, and for security reasons, rupture discs are installed in those spaces where the gas is confined. A rupture disc is a pressure relief device that consists in a metal disk that breaks up at a pre-determined pressure.

The previous step before carrying any process in $scCO_2$ is to chill the gas. Meanwhile, the sample is prepared by placing the reactants in a glass-vial and covering it with filter paper. Then the sample is introduced inside the reactor vessel. The reactor is then closed and connected to its corresponding pipes. The reactor is heated and pressurized to the required pressure and temperature in order to achieve the supercritical regime (all the reactions in this report are carried out at the following conditions: 20 MPa, 70 ºC). Once the reactor has been successfully pressurized and stabilized, it can be isolated from the rest of the system by closing valve V4 and leaving it overnight, so the reaction is performed in batch. Gentle agitation is used to facilitate the physical contact of the reagents.

The residual volume of carbon dioxide in pipes and pump may be released by opening valve V3. At the end of each experiment, the system is slowly depressurized (V5) and allowed to cool down to room temperature.

6.3. PREPARATION OF MOFS

MOFs were prepared from the reaction of a metal salt, organic ligands and additives. Copper(II) nitrate trihydrate ($Cu(NO_3)_2 \cdot 3H_2O$, 99%) and zinc acetylacetonate ($Zn(acac)_2 \cdot xH_2O$) hydrate were chosen as the metal source. 1,3,5-Benzenetricarboxylic acid (H_3BTC, 95%) and 2-methylimidazole (H_2(2-mIm), 99%) were used as the linkers. All reagents were purchased from Sigma-Aldrich and used without further purification. Liquid carbon dioxide (99.995%) was provided by Carburos Metalicos S.A., Air Products Group (Spain).

6.3.1. Preparation of HKUST-1 ($Cu_3(BTC)_2 \cdot 3H_2O$)

1,3,5-Benzenetricarboxylic acid (200.0 mg, 0.83 mmol), copper nitrate trihydrate (115.9 mg, 0.55 mmol) and an additive were placed in a 15 mL-glass vial and charged with a magnetic stirring bar. The sample was allowed to react for 20 h using the supercritical method mentioned above at 20 MPa and 70 ºC. After depressurization and cooling down to room temperature a blue slurry was obtained. In order to eliminate any possible by-products or starting materials, the sample was filtered under vacuum and rinsed with methanol and ethanol. The final product was obtained as a dry blue-turquoise fine powder. Yield: 64%.

Elemental analysis calculation for HKUST-1 fits the formula $(Cu_3(BTC)_2 \cdot 3H_2O) \cdot 3MeOH \cdot H_2O$: Calculated: C, 35.08%; H, 2.80 %. Found: C, 34.90%; H, 2.80%.

6.3.2. Preparation of ZIF-8 ($Zn(2\text{-mIm})_2$)

2-Methylimidazole (150.7 mg, 1.8 mmol), zinc acetylacetonate hydrate (94.0 mg) and an additive were deposited in a 15 mL-glass vial and allowed to react at 20 MPa, 70 ºC for 20 h following the same methodology as for HKUST-1.

Once the experiment was completed the resulting white slurry was filtered under vacuum and rinsed with methanol and ethanol. A white dry powder was finally collected. Yield: 93%.

Elemental analysis calculation for ZIF-8 corresponds to the formula $Zn(2\text{-mIm})_2 \cdot 0.5$ MeOH: Calculated: C, 41.91%; H, 4.97%; N, 23.0%. Found: C, 41.40%; H, 4.48%; N, 22.48%.

7. RESULTS AND DISCUSSION

In this report a new procedure for the synthesis of three dimensional MOFs is presented. Up-to-date the use of supercritical carbon dioxide in the field of MOFs has been limited to the post-synthesis activation, which consists in the removal of solvent molecules that remain in the MOF network after the synthesis, by treating the sample with a flow of $scCO_2$.[18] This procedure can exponentially increase the surface area of the obtained materials.

The supercritical methodology applied in this research work represents the milestone of replacing organic solvents from conventional solvothermal synthesis by the use of supercritical carbon dioxide. Our approach consists on using $scCO_2$ as reaction media for the preparation of previously reported and well-known MOFs, and represents a step-forward in the search for alternative green synthetic methods that do not rely on the use of hazardous organic solvents.

7.1 CHARACTERIZATION OF HKUST-1

7.1.1. X-ray diffraction

Analysis of the synthesized material by X-ray powder diffraction (fig. 12) revealed that the solid was pure HKUST-1 by comparison with the simulated pattern. The former was based on the experimental crystal structure obtained via conventional solvothermal method by Chui et al.[5] In the samples prepared under $scCO_2$, there was no evidence of the presence of crystalline starting materials or by-products.

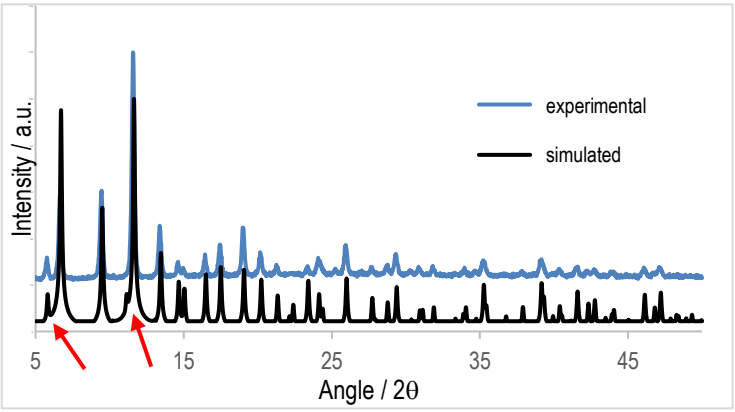

Figure 12. X-ray powder diffraction patterns of HKUST-1. Simulated pattern is in black, experimental pattern is in blue.

Although the overall agreement of the peaks is good, there are some deviations in the relative intensities of two peaks, 2θ = 5.7º and 2θ = 11.2º (see above in Fig.12, marked with red arrows) which are attributed to the degree of hydration of the material. [4]

7.1.2. Thermogravimetric analysis

The thermal stability of this sample was studied using thermogravimetric analysis under air atmosphere (fig. 13).

A gradual and continuous mass loss of 15 % up to a temperature of 300 ºC occurs, due to the evacuation of water and other solvent molecules. Then, between 300-315 ºC a sudden weight-loss step is related to the total decomposition of the material and the elimination of the organic part, confirming the stability of the framework at high temperatures. The remaining product has been reported as copper(II) oxide. [19]

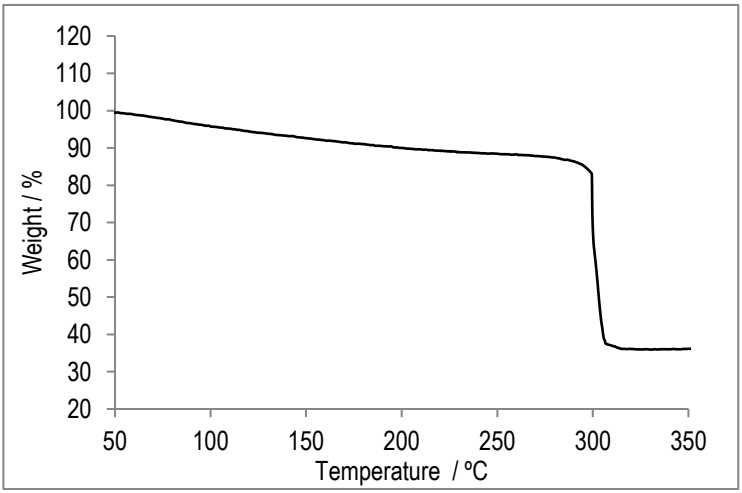

Figure 13. TGA curve for the HKUST-1 MOF obtained under supercritical carbon dioxide.

7.1.3. Scanning electron microscopy

SEM images were obtained to study the morphology and crystallinity. Figures 14 a) and b) correspond to the as-synthesized material (taken from the reactor vessel after the reaction came to an end, and without rinsing with methanol and ethanol) and to the washed product respectively. In fig. 14 a), unreacted chemicals and additives remain in the surface of the product, impeding the visualization of the crystal. The washing step removes such materials and therefore in fig. 14 b) the typical HKUST-1 octahedral shaped-crystals are presented with smooth surface (20.000x magnification). Some crystals have sizes 3-4 μm. Nevertheless, most of the crystals are much smaller, with sizes below 1 μm.

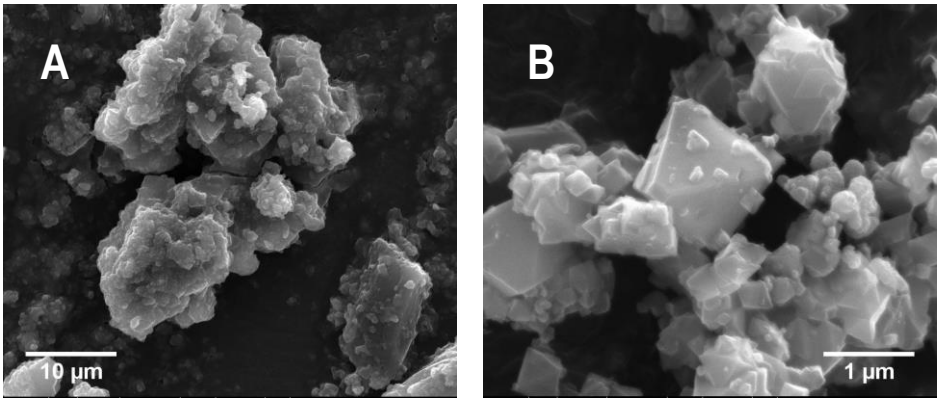

Figure 14. SE-SEM images. a) As synthesized HKUST-1. b) Washed HKUST-1.

The corresponding BSE-SEM images are presented in figures 15 a) and b). The washed HKUST-1 (fig. 15 b) presents a homogeneous phase that corresponds to the MOF structure due to the absence of contrast. The metallic centres and linkers cannot be differentiated for their atomic number due to the resolution of the microscope (would require the use of Scanning Transmission Electron Microscopy, STEM). For analysing the as-synthesized material, the attention is drawn into the area marked with a red square. Different regions with brighter and darker contrast can be observed, which may be attributed to different phases presented on the sample, including starting materials.

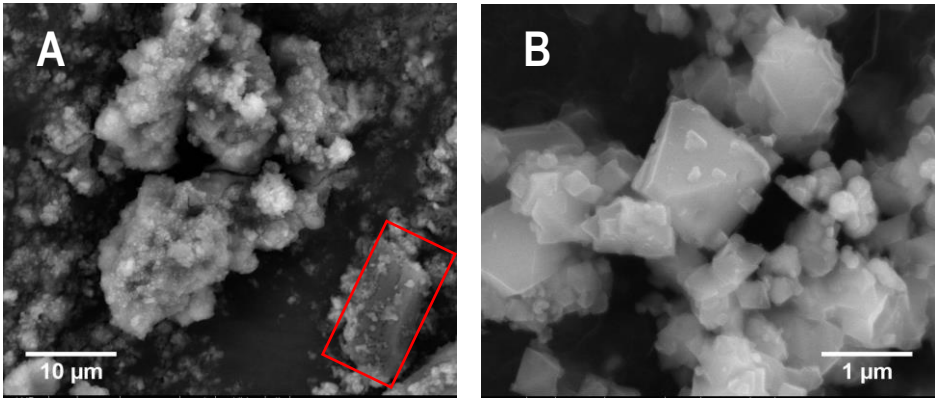

Figure 15. BSE-SEM images. a) As synthesized HKUST-1. b) Washed HKUST-1.

7.1.4. Surface area and pore distribution

Measured BET surface area was 1290 $m^2 \cdot g^{-1}$. This value is within the range of those reported previously in the literature. The observed isotherm (fig. 16) belongs to a Type I according to the IUPAC classification.[16] This is characteristic of physisorption for microporous materials. This fact is confirmed by the pore size distribution diagram that shows how the major pore distribution lies within the micropore region (fig. 17).

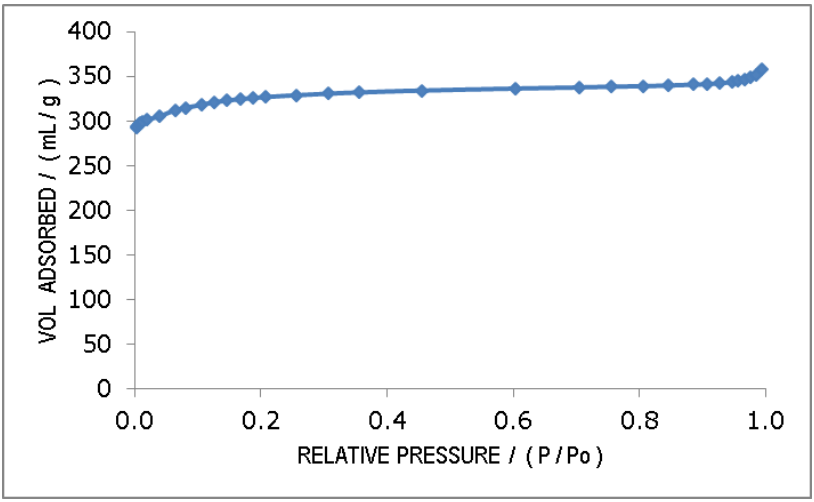

Figure 16. Nitrogen adsorption isotherm of HKUST-1 at 77 K.

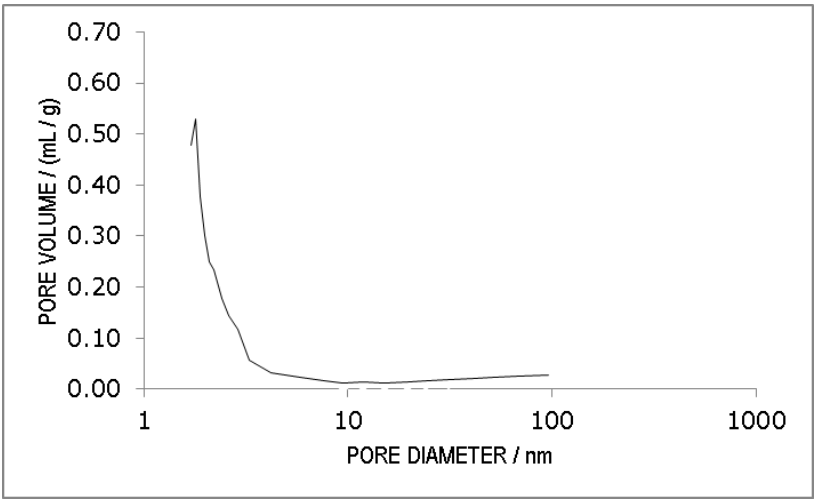

Figure 17. Adsorption pore volume plot for the HKUST-1 material.

7.2 CHARACTERIZATION OF ZIF-8

7.2.1. X-ray diffraction

Comparison of the XRD pattern for the sample (fig. 18) obtained using the supercritical method with the simulated pattern from the reported ZIF-8 single crystal structure, indicates that the obtained product is pure-phase ZIF-8 material.

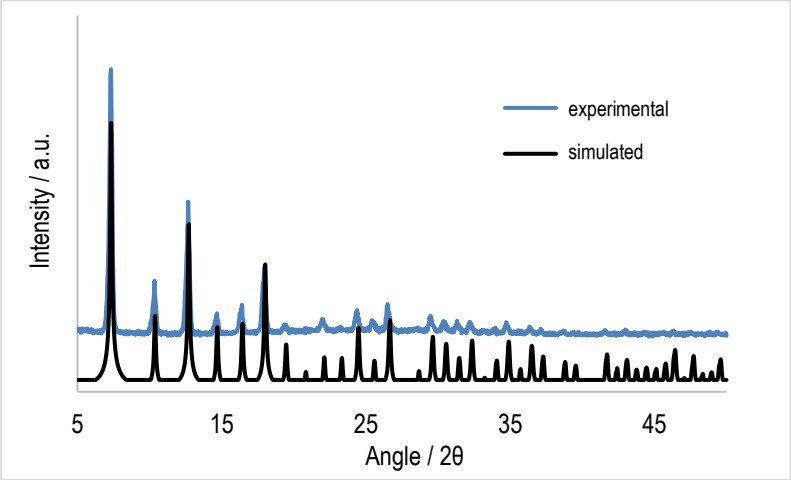

Figure 18. X-ray powder patterns of ZIF-8. Simulated pattern is in black, experimental pattern of synthesized ZIF-8 is in blue.

7.2.2. Thermogravimetric analysis

Figure 19 represents the profile of the thermogravimetric analysis conducted under air atmosphere. From 25 ºC to 300 ºC, the curve exhibits a continuous weight loss of around 15 % corresponding to the removal of solvent molecules. The second event, taking place within the temperature range between 300-320 ºC, correlates with the decomposition of the bridging ligand and therefore the total decomposition of the MOF into zinc(II) oxide. [20]

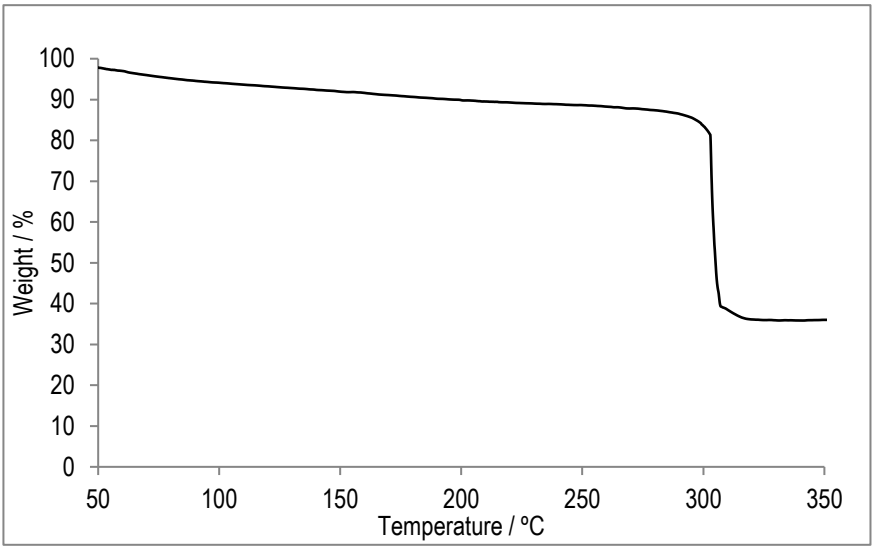

Figure 19. TGA profile for the ZIF-8 MOF obtained under supercritical carbon dioxide.

7.2.3. Scanning electron microscopy

The morphology and particle size of the ZIF-8 sample was evaluated by analysing the obtained SEM images. The sample is mainly constituted by ZIF-8 crystal aggregates like the ones shown in fig. 20. Although a close observation shows a set of different shapes, most of particles adopt a rhombic dodecahedron shape with an average particle size in the range of 500 nm-1 μm. Other available morphologies can be related to the time of growth of the crystals. As shown in figure 21, ZIF-8 crystals are known to evolve from cubic-shaped on a first stage to the final rhombic dodecahedron observed in the SEM microphotograph.[20]

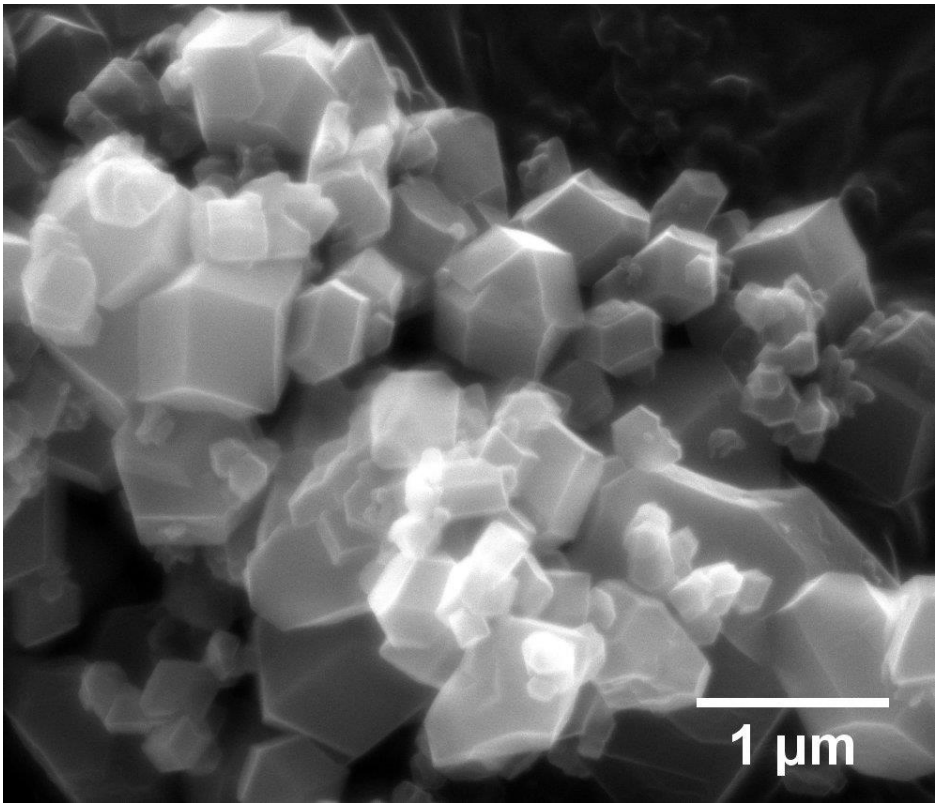

Figure 20. SEM microphotograph of ZIF-8 material.

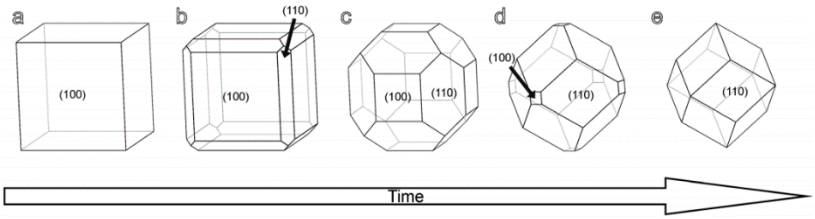

Figure 21. Evolution of ZIF-8 crystal morphology with time: cube (a), cube with truncated edges (b), rhombic dodecahedron with truncated corners (truncated rhombic dodecahedron) (c and d) and rhombic dodecahedron (e).[20]

7.2.4. Surface area and pore distribution

ZIF-8 exhibits a type I nitrogen adsorption isotherm (fig. 22), which reveals its microporous nature. This fact is confirmed by the BJH pore distribution (fig. 23), in which the maximum is located below 1.5 nm (upper limit of the microporous regime) A surface area of 1730 $m^2 \cdot g^{-1}$ was calculated using the BET model. This value surpasses most of other synthetic approaches for the synthesis of this material. [9,20]

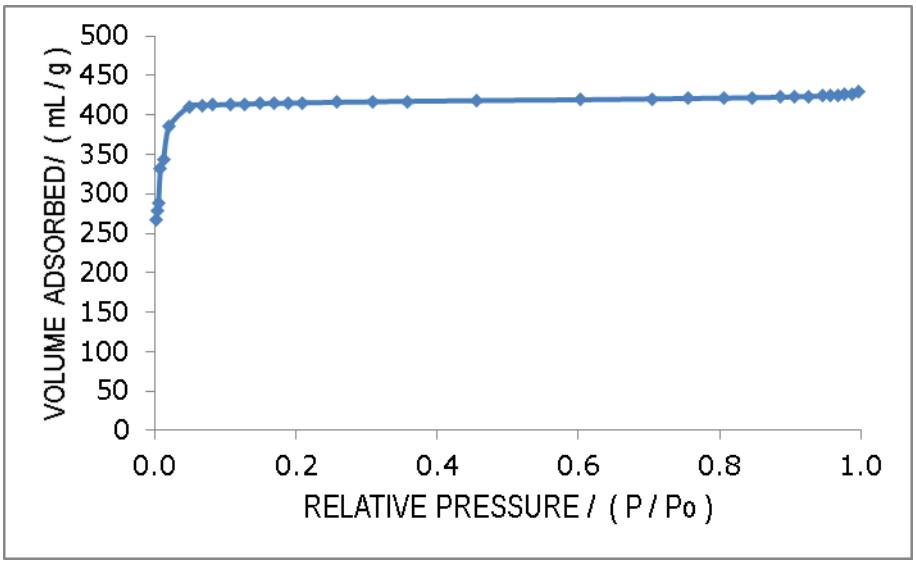

Figure 22. Nitrogen adsorption isotherm of ZIF-8 at 77 K.

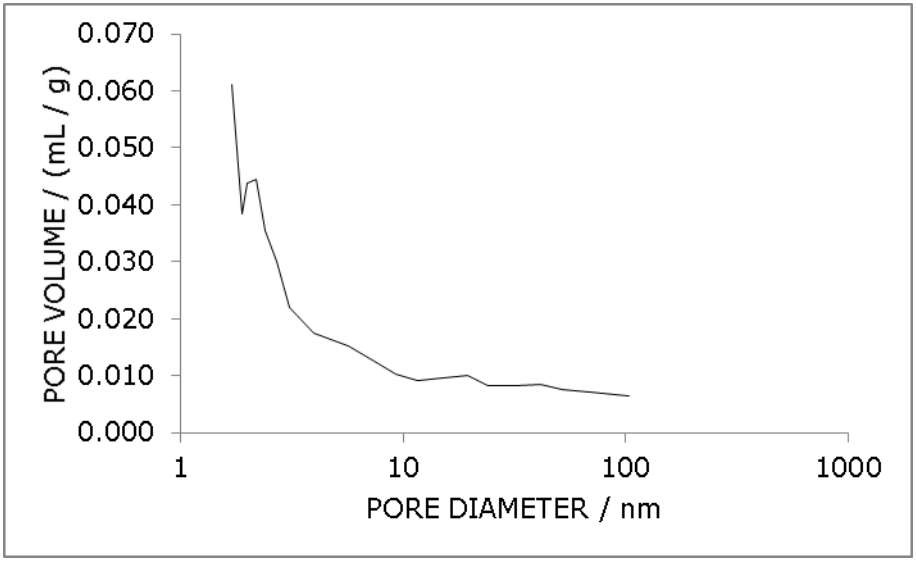

Figure 23. Adsorption pore volume plot for the ZIF-8 material.

7.3 COLOUR CHANGE IN HKUST-1

7.3.1. Experimental observations. Introduction

After performing the BET analysis of HKUST-1, the collected sample presented a deep purple colour (fig. 24 A) contrasting to the original blue-turquoise (fig. 24 B), which returns to the initial coloration by exposing the sample to air. Powder XRD (fig. 25) confirmed that the after-BET material was also HKUST-1, and therefore that removing solvents do not affect to the crystallinity of the material, something that indeed happens with the zinc analogue that collapses into an amorphous structure upon solvent removal.[21] The observed behaviour has been previously reported in literature [22] but an accurate explanation remains necessary.

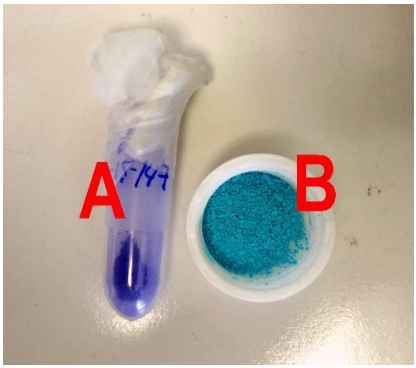

Figure 24. Colour of after-BET (A) and as-synthesized (B) HKUST-1.

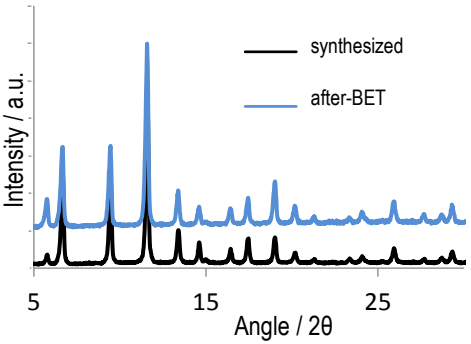

Figure 25. PXRD pattern of synthesized (black) and after-BET (blue) HKUST-1 material.

The Crystal Field Theory (CFT) provides useful information to rationalize the spectrums, stability and magnetic properties of transition metal compounds. Here, it is presented an interpretation based on the analysis of literature UV-Vis spectrums and relating the colour shift to the mentioned theory. In brief, CFT is an electrostatic model that considers the ligands as punctual charges. The repulsion with the metal electrons results in a splitting diagram of the metal d orbitals into groups with different energies[23], like the ones shown in fig. 27 B. The electronic transitions between those levels of energy are known as d-d transitions, which are responsible for the colour in most transition metal compounds. The required amount of energy depends on many factors as for example the metal ion, the geometry, the oxidation state and the nature of the ligands. However, these electronic transitions must obey in all cases to the following selection rules:

- A change in the spin multiplicity is forbidden (Spin selection rule).
- If there is an inversion centre, the parity must be conserved through the transition (Laporte selection rule).

Figure 26 corresponds to the literature reported spectra[22] of synthesized HKUST-1 (full curve) after outgassing at room temperature (dotted curve) and by vacuum treatment at 453 K (dashed curve). The latter would be the most similar situation to the after-BET material (fig. 24 A), as the outgassing procedure includes heating at 60 ºC under high-vacuum for 20 hours.

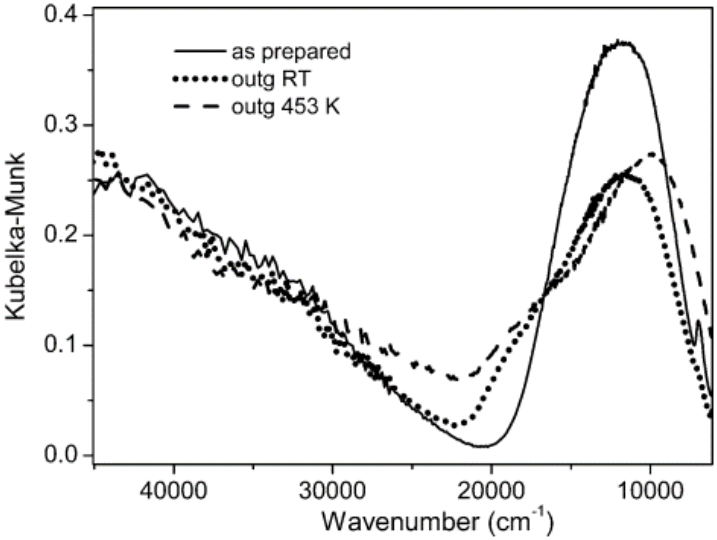

Figure 26. Literature UV-Vis spectrum of HKUST-1 material as-synthesized (full curve), after outgassing at room temperature (dotted curve) and with vacuum treatment at 453 K (dashed curve). [22]

7.3.1. Analyse of Crystal Field Splitting Diagrams

The presented explanation is based on a first study of the crystal field splitting diagram from an octahedral geometry, followed by introducing the special characteristics of HKUST-1 and finalizing with the change in the close surrounding of the copper species as a result of solvent removal and its link to the observed change on colours. For clarity, the variations of the Crystal Field Splitting Diagram are related to d-orbitals, while the d-d transitions (marked with arrows in fig. 27 B) to its corresponding symmetry labels (e.g. a, b, e, t).

The crystal field splitting diagram for a perfect octahedral geometry is represented on figure 27 B.1. Only one d-d transition ($e_g \leftarrow t_{2g}$) is expected due to the degeneracy of the orbitals. The absorption band should be relatively weak as it is forbidden by the Laporte selection rule.

However, the experimental spectrum of the d^9 octahedral ion hexaaquacopper(II) presents a total of two absorptions instead of the single band aforementioned. This is attributed to the Jahn-Teller distortion around the electronic surroundings of the Cu(II) ion that forms a system with lower symmetry. The loss in degeneracy results in the following transitions with the typical energy value given in brackets: [24]

- $b_{1g} \leftarrow e_g$ (12600 cm^{-1})
- $b_{1g} \leftarrow b_{2g}$ (9400 cm^{-1})

The wavelength range of a typical UV-Vis instrument does not register the electronic transition ($b_{1g} \leftarrow a_{1g}$) between the former e_g orbitals from the perfect-octahedral high energy degenerated orbitals.

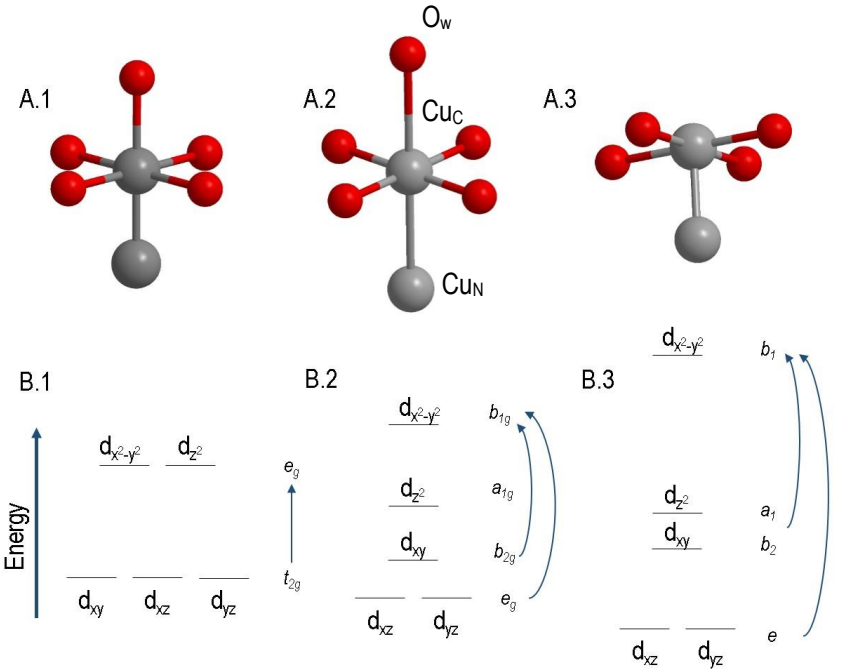

Figure 27. A) Ball and stick model for the octahedral (A.1), distorted octahedral (A.2, which includes labels for some of the atoms) and square-based pyramidal shapes. B) The corresponding Crystal Field splitting diagrams including selected d-d transitions marked with blue arrows.

In the HKUST-1 paddle-wheel environment, the local copper geometry is similar to the one explained in the case of a distorted octahedron. The number of coordination sites for Cu(II) ions has been assumed as six, considering that neighbouring metal atoms occupy one of the coordination sites due to its proximity (Table 1).

Table 1. Selected distances of the local geometry corresponding to the labels in Fig. 26 A.2

	Distance[5] [Å]
$Cu_C \cdots Cu_N$	2.628
Cu-OCO	1.952
$Cu\text{-}OH_2$	2.165

There are two special characteristics in HKUST-1 compared to the distorted octahedron:

- The distance $Cu_c \cdots Cu_N$ is larger than the $Cu\text{-}OH_2$ (Table 1)
- The oxygen atoms from the equatorial ligands do not seem to form a plane.[21]

This situation triggers a different splitting diagram, with the equatorial linkers causing a net stabilization of the d_{xy} orbital and a destabilization of the d_{xz} and d_{yz} orbitals due to a variation of repulsions alongside the metal equatorial oxygen bond. As a result, the d_{xy}, d_{xz}, d_{yz} orbitals lie closer in terms of energy and consequently the expected two absorption bands are seen as a single broad band in the spectrum of the hydrated compound, (figure 25). The great intensity of the band is ascribed to the loss of the inversion centre, and therefore the obligation to follow the Laporte selection rule.

The removal of the coordinated water molecule emerges on a square pyramidal geometry around the metal ion (fig. 27 A.3) and with the internuclear Cu-Cu distance being significantly reduced.[21] A possible crystal field splitting diagram is represented in figure 27 B.3.

The new arrangement can be formally derived from the initial distorted situation. Removing a ligand that was lying along the z axis, results in a great stabilization of the d_{z^2} orbital. On a smaller extent, the energies of the dyz and dxz orbitals are also lowered. The increase in the energy of the $d_{x^2-y^2}$ is not as straightforward. The proximity of the neighbour copper atom results in more repulsions along the plane and therefore a destabilization of that orbital. As a result, the band gap involved in the b1←e (fig. 27 B.3) transition has been significantly increased. This explains the appearances of a high-energy shoulder in the d-d band located at around 18400

cm^{-1} (dotted curve on figure 26). Also, the shift of the maximum to lower energy positions can be explained from the rest of transitions from intermediate energy levels; b1←b2 and b1←a1 (fig. 27 B.3).

The macroscopic effect is a change on the colour of the product. To rationalize the effect of removing a coordinated water molecule, attention must be fixed on the colour of the absorbed light instead of the transmitted (the observed colour). The relation between them is easily stablished with the colour wheel (Table 2) as complementary colours lie opposite to each other across a circle diameter.

The change from blue to violet leads to transitions requiring radiation with greater wavenumbers and therefore more energy (wavenumber and energy are directly related by the Plank's law). This is in accordance with the increase on the band gap as a result of a change in the local geometry of copper ions.

Table 2. Visible part of the electromagnetic spectrum. [23]

Colour of absorbed light	**Approximate wavelengths** [nm]	**Colour of transmitted light**	**Colour wheel representation**
Red	700-620	Green	
Orange	620-580	Blue	
Yellow	580-490	Violet	
Green	560-490	Red	
Blue	490-430	Orange	
Violet	430-380	Yellow	

8. CONCLUSIONS

The developed supercritical method has been successfully proven as an effective strategy for the synthesis of high-crystalline and porous materials, and therefore achieving the goal of introducing greener solvents in the preparation of MOFs. The use of $scCO_2$ enables the establishment of a new, safe and environmentally-friendly route, which may be taken into account for the possible intensification and scale-up to industrial quantities.

In relation to the obtained products, the following conclusions may be considered:

- The materials are obtained as a one high-purity phase, with some solvent molecules remaining in the pore structure.
- The removal of solvent molecules in HKUST-1 results in a colour change from blue to violet, ascribed to an increase on the band gap of the involved d-d transitions.
- The crystal structure and morphology corresponds to that previously reported in literature.
- The synthesized products require a washing step to remove unreacted chemicals.
- Both materials are stable up to temperatures of 300 ºC.
- The surface area values obtained with $scCO_2$ are within the range of other previous synthetic procedures or even overpass those values.

9. REFERENCES AND NOTES

(1) Rouquerolt, J.; Avnir, D.; Fairbridge, C. W.; Everett, D. H.; Haynes, J. H.; Pernicone, N.; Ramsay, J. D. F.; Sing, K. S. W.; Unger, K. K. *Pure Appl. Chem.* **1994**, *66* (8), 1739–1758.

(2) Rowsell, J. L. C.; Yaghi, O. M. *Microporous Mesoporous Mater.* **2004**, *73* (1-2), 3–14.

(3) Zhou, H. C.; Long, J. R.; Yaghi, O. M. *Chem. Rev.* **2012**, *112* (2), 673–674.

(4) Schlichte, K.; Kratzke, T.; Kaskel, S. *Microporous Mesoporous Mater.* **2004**, *73* (1-2), 81–88.

(5) Chui, S. S. Y.; Lo, S. M. F.; Charmant, J. P. H.; Orpen, a G.; Williams, I. D. *Science (80).* **1999**, *283*, 1148–1150.

(6) Tranchemontagne, D. J.; Mendoza-Cortés, J. L.; O'Keeffe, M.; Yaghi, O. M. *Chem. Soc. Rev.* **2009**, *38* (5), 1257–1283.

(7) Phan, A.; Doonan, C. J.; Uribe-Romo, F. J.; Knobler, C. B.; Okeeffe, M.; Yaghi, O. M. *Acc. Chem. Res.* **2010**, *43* (1), 58–67.

(8) Huang, X.-C.; Lin, Y.-Y.; Zhang, J.-P.; Chen, X.-M. *Angew. Chem. Int. Ed. Engl.* **2006**, *45* (10), 1557–1559.

(9) Park, K. S.; Ni, Z.; Côté, A. P.; Choi, J. Y.; Huang, R.; Uribe-Romo, F. J.; Chae, H. K.; O'Keeffe, M.; Yaghi, O. M. *Proc. Natl. Acad. Sci. U. S. A.* **2006**, *103* (27), 10186–10191.

(10) Atkins, P.; Paula, J. De.-, **2009**, *Physical Chemistry*; Ninth Edition, W.H. Freeman.

(11) Beckman, E. J. *J. Supercrit. Fluids* **2004**, *28* (2-3), 121–191.

(12) Capello, C.; Fischer, U.; Hungerbühler, K. *Green Chem.* **2007**, *9* (9), 927.

(13) Goodhew, P. J.; Humphreys, J.; Beanland, R.; **2000** *Electron Microscopy and Analysis, Third Edition*, Taylor & Francis.

(14) Reed, S. J. B.; **2005,** *Electron Microprobe Analysis and Scanning Electron Microscopy in Geology*; Cambridge University Press.

(15) K.S. Walton, R. Q. S. *J. Am. Chem. Soc.* **2007**, 129, 8552–8556.

(16) Condon, J. B.; **2006**, *Surface Area and Porosity Determinations by Physisorption*; Elsevier.

(17) Barrett, E. P.; Joyner, L. G.; Halenda, P. P. *J. Am. Chem. Soc.* **1951**, *73* (1), 373–380.

(18) Nelson, A. P.; Farha, O. K.; Mulfort, K. L.; Hupp, J. T. *J. Am. Chem. Soc.* **2009**, *131* (2), 458–460.

(19) Lin, K.-S.; Adhikari, A. K.; Ku, C.-N.; Chiang, C.-L.; Kuo, H. *Int. J. Hydrogen Energy* **2012**, *37* (18), 13865–13871.

(20) Schejn, A.; Balan, L.; Falk, V.; Aranda, L.; Medjahdi, G.; Schneider, R. *CrystEngComm* **2014**, *16* (21), 4493.

(21) Bhunia, M. K.; Hughes, J. T.; Fettinger, J. C.; Navrotsky, A. *Langmuir* **2013**, *29* (25), 8140–8145.

(22) Prestipino, C.; Regli, L.; Vitillo, J. G.; Bonino, F.; Damin, A.; Lamberti, C.; Zecchina, A.; Solari, P. L.; Kongshaug, K. O.; Bordiga, S. *Chem. Mater.* **2006**, *18* (5), 1337–1346.

(23) Housecroft, C. E.; Sharpe, A. G.; **2004**, *Inorganic chemistry*; Second edition, Pearson Education.

(24) Sutton, D.; **1975**, *Espectros electrónicos de los complejos de los metales de transición*; Reverté.

10. ACRONYMS

2-mIm: 2-methylimidazolate.

a.u.: Arbitrary Units.

BET: Brunauer, Emmett and Teller.

BSE: Backscattered Electrons.

BTC: 1,3,5-bencenetricarboxylate.

CCDC: Cambridge Crystallographic Data Centre.

CFT: Crystal Field Theory.

DEF: Diethylformamide.

DMF: Dimethylformamide.

IUPAC: International Union of Pure and Applied Chemistry.

MOF: Metal-Organic Framework.

PXRD: Powder X-ray diffraction

SBU: Secondary Building Unit.

$scCO_2$: Supercritical carbon dioxide.

SCF: Supercritical Fluid.

SE: Secondary Electrons.

SEM: Scanning Electron Microscopy.

STEM: Scanning Transmission Electron Microscopy.

TGA: Thermogravimetric analysis.

UV-Vis: Ultraviolet-Visible.

ZIF: Zeolitic Imidazole Framewoks.